XPS and UPS Valence Band Studies
of Nanocrystalline Ni-Ti Alloy Thin Films

S. Pacanowski[a], J. Skoryna[a,*], A. Szajek[a], A. Marczyńska[a], H. Dawczak-Dębicki[a,b],
M. Werwiński[a] and L. Smardz[a]

[a]Institute of Molecular Physics, Polish Academy of Sciences, M. Smoluchowskiego 17, 60-179 Poznań, Poland
[b]Faculty of Physics, Adam Mickiewicz University, Umultowska 85, 61-614 Poznań, Poland
[c]Wielkopolska Centre of Advanced Technologies, Adam Mickiewicz University,
Umultowska 89C, 60-614 Poznań, Poland

In this contribution we study valence bands of *in-situ* prepared nanocrystalline NiTi and Ni_3Ti alloy thin films using X-ray and ultraviolet photoelectron spectroscopy. Additionally, theoretical valence band of NiTi alloy was calculated by *ab-initio* methods. The structure and morphology of the samples were studied by X-ray diffraction and atomic force microscopy, respectively. Furthermore, hydrogen absorption and desorption kinetics at a pressure of about 1000 mbar were studied in Pd covered nanocrystalline NiTi alloy thin film using four-point resistivity measurements. Results showed that modifications of the valence bands of the Ni-Ti thin films due nanocrystalline structure can influence on the room temperature hydrogen absorption and desorption kinetics.

1. Introduction

Conventional metal hydrides have the advantages of proper volumetric density, relatively low working pressure, and a reasonable reversibility [1]. In particular, MgH_2 has attracted a lot of attention as a solid-state hydrogen storage medium due to its high gravimetric capacity (7.6 wt %) and encouraging reversibility [2, 3]. However, the main disadvantages preventing the commercial application of Mg are its high thermodynamic stability, high dehydrogenation temperature and slow kinetics. Many investigations have been carried out to decrease the operation temperature and improve the kinetics through grain size control [4]. Traditional energetic ball milling and cold rolling result in improved hydrogen storage properties because they decrease the grain size, and introduce defects which provide rapid diffusion paths for hydrogen and reduce the diffusion distances [5].

Thin films offer an opportunity to carry out studies on aspects such as average grain size, shape of the interfaces, and composition, because these can be accurately tailored on the nanoscale [6, 7]. During the growth process of thin films average grain size can increase starting from the substrate interface, resulting with many grain boundaries in such samples [8]. Dislocations and vacancies are present in higher density than in bulk material. Even when the grain size is maximized by epitaxial film growth, dislocations are generated during the growth process to adjust for the lattice mismatch between the film and the substrate [9]. The local hydrogen affinity is different for these defects and therefore the materials properties are expected to be influenced by all these microstructural components.

Furthermore, it is well known, that properties of the nanoparticles change due to the size and surface induced modifications of the electronic structures [10, 11]. Materials properties are strongly affected by microstructural contributions, therefore the microstructure can be used to tune materials properties for applications. For example, the electrochemical hydrogen properties of NiTi - based alloys could be improved by ball milling and annealing [12]. Because of remarkable shape memory effect, pseudoelasticity, corrosion resistance, biocompatibility and excellent mechanical properties [13], the NiTi based alloys have also attracted considerable attention in recent years as functional materials in aerospace engineering, intelligence control, medical implants, etc. In this paper we study experimentally valence bands of nanocrystalline NiTi and Ni_3Ti alloy thin films using *in-situ* X-ray (XPS) and ultraviolet (UPS) photoemission spectroscopy. XPS valence band measured for nano-crystalline NiTi thin film was compared to that obtained for ideal single-crystalline alloy using *ab-initio* calculations. Hydrogen absorption and desorption kinetics were studied in Pd covered NiTi thin film at room temperature (RT).

2. Experimental and calculations methods

Nanocrystalline Ni-Ti alloy thin films were prepared onto oxidised Si(100) substrates at RT using ultra high vacuum (UHV) magnetron co-sputtering [14-16]. Ni (99.998 at. %) and Ti (99.99 at. %) targets were sputtered using DC and RF modes, respectively. The total thickness of the alloy thin film samples was about 100 nm. The base pressure before the deposition process

---

*corresponding author; e-mail: jskoryna@ifmpan.poznan.pl

was lower than 5×10^{-10} mbar. As a substrate we have used Si(100) wafers with an oxidised surface to prevent a silicide formation. Therefore, we have applied a special heat treatment in UHV before deposition in order to obtain an epitaxial SiO$_2$ surface layer [17]. The structure and morphology of the samples have been studied by X-ray diffraction (XRD) and atomic force microscopy (AFM), respectively. The chemical composition and the cleanness of all layers was checked *in-situ*, immediately after deposition, transferring the samples to the analysis chamber (5×10^{-11} mbar) equipped with XPS and UPS. We have used Al-K$_\alpha$ (1486.6 eV) and He-I (21.2 eV) radiation in the XPS and UPS measurements, respectively. Details of the XPS experiments can be found in Refs. [18-21]. Furthermore, hydrogen absorption and desorption kinetics at RT at a pressure of about 1000 mbar were studied in NiTi (covered by 10 nm – Pd) thin film using four-point resistivity measurements.

The fully relativistic calculations were carried out based on the full-potential local-orbital minimum-basis scheme FPLO (FPLO-14.00-49) [22] with the generalized gradient approximation (GGA) in the Perdew-Burke-Ernzerhof (PBE) form [23]. The calculations were performed for the reciprocal space mesh containing 1771 k-points within the irreducible wedge of the Brillouin zone. The self-consistent convergence criteria were equal to 10^{-8} Ha for the total energy and for a charge density of 10^{-6}. The theoretical XPS spectra were obtained from the calculated densities of electronic states convoluted by Gaussian with a half-width (δ) equal to 0.5 eV and scaled using the proper photo-electronic cross sections for partial states [24].

3. Results and discussion

In Fig. 1 we show AFM image (1 μm $\times$ 1 μm) of 100 nm – TiNi thin film. The roughness parameter R_a calculated from greater area (2 μm $\times$ 2 μm) was as small as 0.11 nm. Average grain size was estimated as 35 nm.
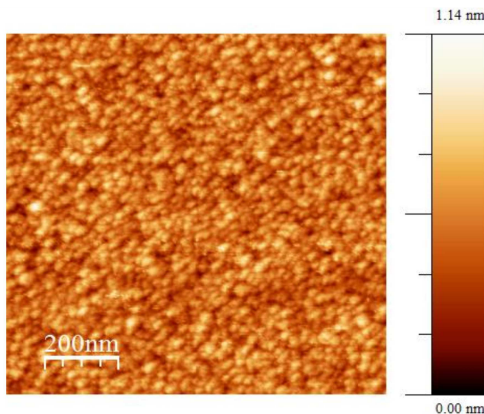
Fig. 1. AFM image of nanocrystalline NiTi alloy thin film.
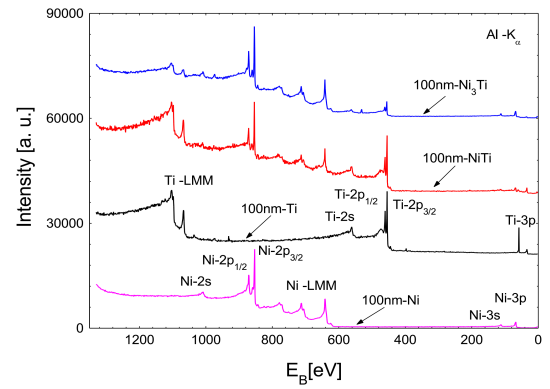
Fig. 2. XPS spectra (Al-K$_\alpha$) of *in-situ* prepared Ni, Ti, and nanocrystalline NiTi and Ni$_3$Ti alloy thin films.
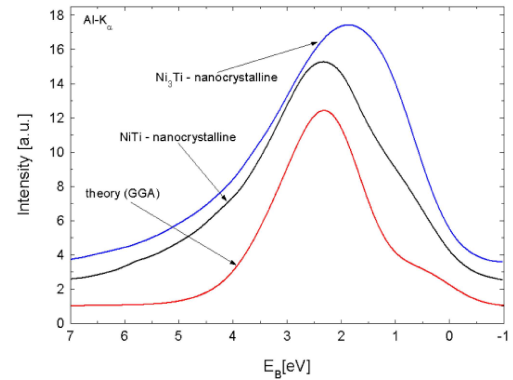
Fig. 3. Experimental XPS valence band spectra of nanocrystalline NiTi and Ni$_3$Ti alloy thin films. For a comparison we also show XPS valence band spectra calculated for single-crystalline NiTi.

Experimental XPS core-level spectra for the freshly prepared nanocrystalline NiTi and Ni$_3$Ti alloy thin films are shown in Fig. 2. For a comparison we also show XPS spectra for pure Ni and Ti thin films. The total thickness of all the prepared thin film samples was about 100 nm. Due to well known high reactivity of titanium with oxygen we have prepared the nanocrystalline alloy thin films after an additional heating of the sample holder and substrate at 700 K for 3 h and cooling to 293 K under UHV conditions. Results showed that after such an outgassing procedure, it is possible to prepare oxygen- and carbon-free surface. The oxygen and other impurities are absent on the surface of such prepared thin films. Practically no XPS signal from potential contamination atoms like O-1s and C-1s is observed (see Fig. 2). On the other hand, we have observed oxygen atoms (~ 1 at.%) already adsorbed on Ti based alloy thin film surfaces 3h after preparation despite the UHV.

In Fig. 3 we show experimental XPS valence band spectra of nanocrystalline NiTi and Ni$_3$Ti alloy thin films. For a comparison we also show XPS valence band spectra calculated for single-crystalline NiTi alloy within GGA.

As can be observed, the positions of the experimental spectrum measured for the nanocrystalline NiTi thin film is practically the same as for theoretical XPS spectra. However, the XPS valence band measured for the nanocrystalline sample is considerably broadened compared to those determined by ab-initio calculations (see Fig. 3) or measured for the polycrystalline bulk material [25]. Note that the theoretical calculations were performed for the perfect single-crystal structure. Therefore, the broadening of the experimental valence band could be explained by the specific nanostructure of the thin film samples [18-21]. Such a modification of the valence bands of nanocrystalline materials based on Ni-Ti alloys could significantly improve the discharge capacity [26].
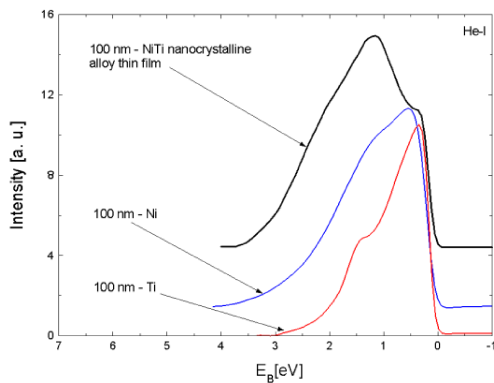
Fig. 4. UPS (He I) valence band spectra of pure Ni and Ti thin films and nanocrystalline NiTi and Ni$_3$Ti alloy thin films.
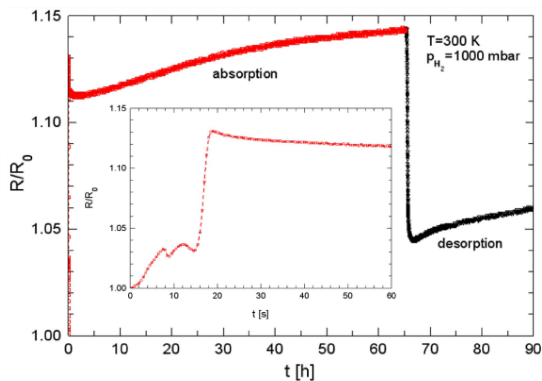
Fig. 5. Hydrogen absorption/desorption kinetics for nanocrystalline 100nm-NiTi alloy thin film. Relative resistance was measured using four-point method at room temperature. The inset shows the first 60 s of the hydrogen absorption.

Figure 4. shows the experimental UPS valence band spectrum of nanocrystalline NiTi alloy thin film. For a comparison we also show UPS valence band spectra measured for pure Ni and Ti thin films. As can be observed, the spectrum measured for the nanocrystalline NiTi thin

film is also slightly shifted and broadened compared to that determined for the polycrystalline bulk material [25].

In Fig. 5 we show relative resistivity change of the nanocrystalline 100 nm - NiTi alloy thin film during hydrogen absorption and desorption at a pressure of about 1000 mbar. Note that immediately after preparation the alloy thin film was covered *in-situ* by 10 nm Pd layer to catalyze hydrogen absorption and to protect against oxidation. The sample shows rather low and two step resistivity change during the first 20 s of RT absorption (see inset in Fig. 5). On the other hand, the polycrystalline 100 nm - NiTi alloy thin film coverd by 10 nm of Pd showed practically no hydrogen absorption (resistivity change). Basing on the *in-situ* XPS studies (not shown here) any possible contaminations at the NiTi/Pd interface can be ruled of as a reason responsible for such an absorption kinetics.

In conclusion, the different microstructure observed in the nano- and polycrystalline NiTi alloy thin film leads to modifications of its electronic structure and as a result can influence on the RT hydrogenation.

Acknowledgments

References

[1] L. Schlapbach, A. Züttel, *Nature* **414**, 353 (2001).

[2] F.E. Pinkerton, B.G. Wicke, *Ind. Phys.* **10**, 20 (2004).

[3] M. Jurczyk, L. Smardz, I. Okonska, E. Jankowska, M. Nowak, K. Smardz, *Int. J. Hydrog. Energy* **33**, 374 (2008).

[4] H. Imamura, K. Masanari, M. Kusuhara, H. Katsumoto, T. Sumi, Y. Sakata, *J. Alloys Compd.* **386**, 211 (2005).

[5] A.D. Rud, A.M. Lakhnik, V.G. Ivanchenko, V.N. Uvarov, A.A. Shkola, V.A. Dekhtyarenko L.I. Ivaschuk, N.I. Kuskova, *Int. J. Hydrog. Energy* **33**, 1310 (2008).

[6] B. Dam, R. Gremaud, C. Broedersz, R. Griessen, *Scr. Mater.* **56**, 853 (2007).

[7] A. Borgschulte, R.J. Westerwaal, J.H. Rector, B. Dam, R. Griessen, *Appl. Phys. Lett.* **85**, 4884 (2004).

[8] M. Ohring, *The Materials Science of Thin Films*, Academic Press, San Diego 1991.

[9] W.D. Nix, *Metall. Trans. A* **20**, 2217 (1989).

[10] S.K. Sengar, B.R. Mehta, L.K. Malhotra, S.M. Shivaprasad, *Appl. Phys. Lett.* **98**, 193115 (2011).

[11] S.K. Sengar, B.R. Mehta, P.K. Kulriya, S.A. Khan, *Appl. Phys. Lett.* **103**, 173107 (2013).

[12] Z. Zhang, O. Elkedim, Y.Z. Ma, M. Balcerzak, M. Jurczyk, *Int. J. Hydrog. Energy* **42**, 1444 (2017).

[13] K. Otsuka, X. Ren, *Prog. Mater. Sci.* **50**, 511 (2005).

[14] L. Smardz, *J. Alloys Compd.* **395,** 17 (2005).

[15] L. Smardz, K. Smardz, H. Niedoba, *J. Magn. Magn. Mater.* **220**, 175 (2000).

[16] L. Smardz, K. Le Dang, H. Niedoba, K. Chrzumnicka, *J. Magn. Magn. Mater.* **140-144**, 569 (1995).

[17] L. Smardz, U. Köbler, W. Zinn, *Vacuum* **42**, 283 (1991).

[18] L. Smardz, M. Nowak, M. Jurczyk, *Int. J. Hydrog. Energy* **37**, 3659 (2012).

[19] K. Smardz, L. Smardz, M. Jurczyk, E. Jankowska, *Phys. Stat. Sol. (a)* **196**, 263 (2003).

[20] L. Smardz, M. Jurczyk, K. Smardz, M. Nowak, M. Makowiecka, I. Okońska, *Renew. Energy* **33**, 201 (2008).

[21] K. Smardz, L. Smardz, I. Okonska, M. Nowak, M. Jurczyk, *Int. J. Hydrog. Energy* **33**, 387 (2008).

[22] K. Köpernik, H. Eschrig, *Phys. Rev. B* **59**, 1743 (1999).

[23] J. P. Perdew, K. Burke, M. Ernzerhof, *Phys. Rev. Lett.* **77,** 3865 (1996).

[24] J. J. Yeh, I. Lindau, *At. Data Nucl. Data Tables* **32**, 1 (1985).

[25] S. Shabalovskaya, A. Narmonev, O. Ivanova, A. Dementjev, *Phys. Rev.* **B48**, 13296 (1993).

[26] A. Szajek, M. Makowiecka, E. Jankowska, M. Jurczyk, *J. Alloys Compd.* **403**, 323 (2005).